Band structure of $La_2NiO_{4.25}$ ($La_8Ni_4O_{17}$)

Antoine Villesuzanne,* Alain Demourgues, Jean-Claude Grenier, Jean-Pierre Doumerc, Alain Wattiaux and Michel Pouchard

Institut de Chimie de la Matière Condensée de Bordeaux, UPR CNRS no 9048, 33608 Pessac, France

The monoelectronic band structures of $La_8Ni_4O_{17}$ at 9 and 300 K are calculated using the extended Hückel tight-binding method. Within a rigid band hypothesis and discussing the location of the Fermi level, we obtain band diagrams which corroborate experimental data such as the evolution of the Curie constant and Ni—O bond length distributions with temperature, as well as the assumptions of (*a*) hopping-type conductivity in narrow bands, with at least two type of carriers, (*b*) a mixed valence for nickel ranging from +I to +III, (*c*) a charge-transfer equilibrium, displaced with temperature, (*d*) the occurrence of $(O_3)^{5-}$ entities ($O_{apex}—O_{interstitial}—O_{apex}$), although the O^{2-} hypothesis for all oxygen ions in the structure can not be excluded within this study.

Due to its similarities with the superconducting cuprate $La_2CuO_{4+\delta}$ and to its capability to accommodate high intercalated oxygen rates δ, the $La_2NiO_{4+\delta}$ series has been extensively studied during the last years, from both structural and electronic properties points of view.[1–6] Transport and magnetic properties of $La_2NiO_{4+\delta}$ ($0 \leqslant \delta \leqslant 0.25$) were reported in a previous paper.[1] The compounds remain semiconducting whatever δ and, for $\delta \geqslant 0.11$, the transport properties were interpreted assuming variable range hopping with at least two types of carriers. The magnetic susceptibility of $La_2NiO_{4.25}$ obeys a Curie–Weiss law below 150 K ($C_M \approx 0.33$ emu K per Ni); an enhancement of the Curie constant at higher temperatures reveals a change in the electronic configuration of nickel ions. Detailed structural and EPR studies for this last compound[7,8] revealed the occurrence of a nickel mixed valence ranging from +I to +III, correlated to a strongly distorted structure; intercalated oxygen atoms (O_i) order within the La_2O_2 layers, leading to the definite compound $La_8Ni_4O_{17}$. The monoclinic cell (*C*2 space group) contains six different nickel sites, described and labelled in Table 1 and Plate 1. The interstitial oxygen exhibits two short bonds with apex oxygen atoms, $d(O_i—O_{apex}) = 2.17$ and 2.25 Å at 9 K, 2.18 and 2.28 Å at 300 K; an analysis based on bond orders and Madelung potentials suggests the existence of $(O_3)^{5-}$ entities in the compound.[8] A charge-transfer mechanism, described by the disproportionation equilibrium (1) (see Table 1 and Plate 1 for Ni ion labels):

$$Ni^+(1) + Ni^{3+}(5 \text{ or } 6) \leftrightarrow Ni^{2+}(1) + Ni^{2+}(5 \text{ or } 6) \qquad (1)$$

and shifted to left-hand side at low temperature, can account for the structural differences in $La_8Ni_4O_{17}$ between low and room temperature.

These experimental features picture the close connection between electronic and crystallographic structures; some advanced hypotheses have been made: occurrence of a mixed valence of nickel involving Ni^+, Ni^{2+} and Ni^{3+}; existence of $(O_3)^{5-}$ entities; contribution of several types of carriers to the

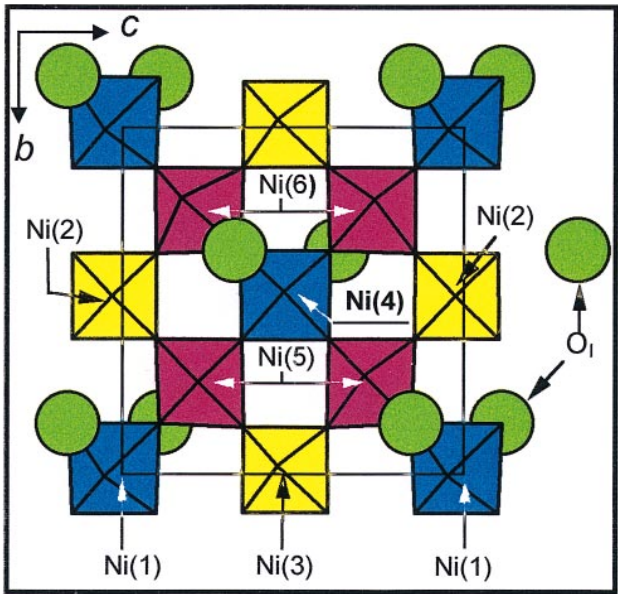

Plate 1 Top view of the $(NiO_4)_8$ layer in $La_8Ni_4O_{17}$, showing the six different sites for Ni ions. Interstitial oxygen atoms are represented.

Table 1 Ni—O bond lengths (Å) of the six nickel sites in $La_8Ni_4O_{17}$ at 9 and 300 K (from ref. 8)

	Ni(1)	Ni(2)	Ni(3)	Ni(4)	Ni(5)	Ni(6)
9 K	1.98(1) × 2	1.88(1) × 2	1.89(1) × 2	1.94(1) × 2	1.84(2)	1.77(2)
	2.00(1) × 2	1.90(1) × 2	1.92(1) × 2	2.01(1) × 2	1.94(2)	1.91(2)
	2.27(1) × 2	2.20(1) × 2	2.23(1) × 2	2.23(1) × 2	1.97(2)	1.98(2)
					2.00(2)	2.01(2)
					2.13(2)	2.18(2)
					2.20(2)	2.23(2)
300 K	1.93(1) × 2	1.90(1) × 2	1.89(1) × 2	1.95(1) × 2	1.85(2)	1.85(2)
	1.96(1) × 2	1.90(1) × 2	1.91(1) × 2	2.01(1) × 2	1.96(2)	1.96(2)
	2.20(1) × 2	2.21(1) × 2	2.20(1) × 2	2.26(1) × 2	1.97(2)	1.99(2)
					1.98(2)	2.01(2)
					2.10(2)	2.13(2)
					2.29(2)	2.31(2)

electrical conductivity and charge-transfer equilibrium with thermal dependence.

It seemed interesting to check whether these hypotheses agreed or not with a band structure calculation using the exact crystallographic structures of $La_8Ni_4O_{17}$, refined at 9 and 300 K.[9] The large unit cell requires a semi-empirical method for the band structure calculation; the results will serve as a basis for discussing the points stressed above. The key point of our approach is keeping the complete structural information during the theoretical study. The use of first principles or *ab initio* methods would require a drastic schematisation of the structure, which would be regrettable as structural and electronic properties seem to be strongly interdependent in $La_8Ni_4O_{17}$.

The strategy of the present work is completely different from the one used in band structure calculations including correlation effects (for example, Anisimov *et al.*[10] included a Hubbard U parameter in the local-density approximation formalism, LDA + U, for the study of $La_{2-x}Sr_xNiO_4$), which can only be applied to unit cells containing a few atoms.

Method of calculation

We used the extended Hückel tight-binding method (EHTB)[11–13] for calculating the monoelectronic band structure of $La_8Ni_4O_{17}$ at 9 and 300 K. A valence atomic orbitals basis set (Slater-type orbitals) is attached to each atom in the unit cell. The EHTB method takes into account the complete crystal structure, *via* the atomic orbital overlap integrals used in the calculation of the effective Hamiltonian matrix elements. The method is not of the self-consistent field type but has been shown to give a description similar to those obtained with more sophisticated methods, at least for states lying close to the Fermi level.[14] It generally leads to quantitative information about those electronic properties governed by the topology of interactions (hybridisations, band shapes, Fermi surfaces).[15–19]

The total and projected density of states (DOS) curves illustrate the influence of the various structural distortions on the band structure, such as band splittings. Another calculated quantity, defined in the framework of the EHTB method,[15,20] is of great interest for the study of crystal *vs.* electronic structures relationships: the crystal orbital overlap population (COOP). The COOP is the extension to the solid of the Mulliken overlap population.[21] It gives the bonding contribution (in sign and magnitude) of crystal orbitals to a given bond. When cumulated up to E_F, COOPs are related both to the distribution of bond lengths and to the stability of the compound.

The guideline of the present study, and the only step beyond the monoelectronic approximation, will consist of the determination of the Fermi level position.[22,23] The rather localised character of 3d states in transition metal oxides may favour the single occupancy of states close to E_F. In an ionic description, this corresponds to the energy competition between high- and low-spin states. In the present approach a rigid band hypothesis is assumed, which implies that the band structure is not drastically affected by the occupancy of bands. The comparison with experimental data is used to determine the E_F position. If a good agreement is found between the experimental features and the electronic structure for a given E_F, *i.e.* for a given band occupancy, the rigid band approximation is considered valid for this study.

Computational aspects

The basis set and related parameters used for lanthanum, nickel and oxygen atoms are reported in Table 2. We used as input geometry the crystallographic structure determined from neutron powder-diffraction data at 9 and 300 K.[9] The primitive triclinic unit cells of $La_8Ni_4O_{17}$ at 9 and 300 K contain two formula units; they are described by a 352 atomic orbitals basis set. As the K_2NiF_4-type structure has a pronounced 2D character, neglecting the translation symmetry perpendicular to the layers could appear as a good approximation, leading to a large gain in computational time and memory. However, the environment of the transition metal layer has to be correctly taken into account. The 2D character of $La_8Ni_4O_{17}$ being less significant than in the basic K_2NiF_4 structure, mainly because of the presence of interstitial oxygen atoms, 3D translation symmetry and reciprocal lattice were used.

Table 2 Extended Hückel parameters (double-ζ expansion is used for Slater-type d orbitals)

element	orbital	H_{ii}/eV	ζ_1
La	5d[a]	−8.21	3.78
	6s	−7.67	2.14
	6p	−5.01	2.08
Ni	3d[b]	−13.49	5.75
	4s	−9.17	1.825
	4p	−5.15	1.825
O	2s	−32.3	2.275
	2p	−14.8	2.275

[a] $c_1 = 0.7765$, $\zeta_2 = 1.381$, $c_2 = 0.4586$. [b] $c_1 = 0.5683$, $\zeta_2 = 2.00$, $c_2 = 0.6292$.

For the integration over the reciprocal lattice primitive cell, the first primitive zone was used instead of the first Brillouin zone.[16] A few k-point grids containing up to 260 points were tested for the coverage of half of the first primitive zone. A 116 k-points grid was finally chosen as no significant changes in energy bands and atomic populations were obtained with denser grids.

The calculations were performed on a CRAY Y/MP-EL computer after adaptation of the program EHMACC (Extended Hückel Molecular and Crystal Calculations, program no. 571 of the Quantum Chemistry Program Exchange). The total and projected DOS, the atomic and overlap populations as a function of E_F were calculated for $La_8Ni_4O_{17}$ at 9 and 300 K.

Results

Before discussing the location of E_F in the band diagrams, some features can be extracted from the total and projected DOS curves. Fig. 1 shows the total DOS as a function of energy for $La_8Ni_4O_{17}$ at 9 and 300 K and for $La_2NiO_{4.00}$ (*Bmab* space group) for sake of comparison. Projected DOS gives the different contributions to the bands, in terms of atoms or atomic orbitals. Fig. 2 focuses on antibonding $3d_{z^2}$ and $3d_{x^2-y^2}$ character bands, that are denoted $\sigma^*_{z^2}$ and $\sigma^*_{x^2-y^2}$ in the following. Global oxygen contribution is plotted and the nickel ions contributing mainly to each band or band stack are indicated. As expected, the relative energies of $\sigma^*_{x^2-y^2}$ bands are governed by in-plane Ni—O bond lengths, *i.e.* by $3d_{x^2-y^2}$–$2p_\sigma$ overlap (Table 1). The case of $\sigma^*_{z^2}$ bands is not so simple because in-plane Ni—O bond lengths play a non-negligible role *via* the overlap between $2p_\sigma$ and the equatorial lobe of $3d_{z^2}$ orbital, though the main contribution is due to apical Ni—O bond lengths (*i.e.* $3d_{z^2}$–$2p_z$ overlap). Compared with the $La_2NiO_{4.00}$ DOS, the $3d_\sigma$* bands partly split because of various types of distortions; it results in very narrow bands with pronounced localised character and separated by band gaps, which suggests that the compound remains non-metallic whatever the location of the Fermi level within the $3d_\sigma$* bands. The lowest energy bands within each band stack ($\sigma^*_{x^2-y^2}$ and $\sigma^*_{z^2}$) are associated with the same type of nickel ions: Ni(1) and Ni(4) at 9 K, Ni(4) and Ni(6) at 300 K; thus, the partial occupancy of $\sigma^*_{x^2-y^2}$ and $\sigma^*_{z^2}$ band stacks will lead to very different electron populations for nickel ions and, as it

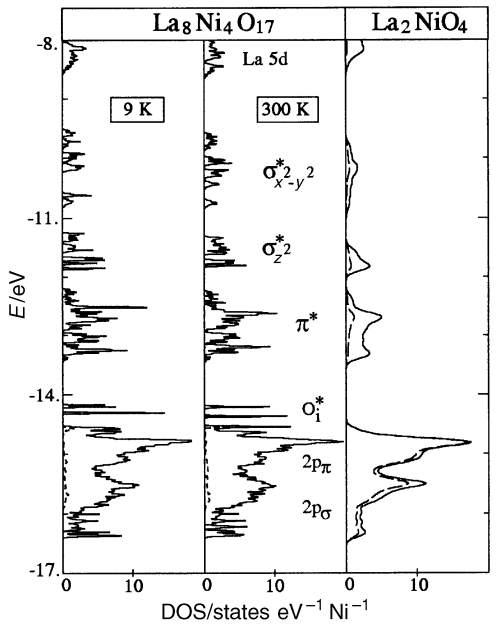

Fig. 1 DOS curves for $La_8Ni_4O_{17}$ at 9 and 300 K, and for $La_2NiO_{4.00}$ (space group *Bmab*). Dotted line shows the interstitial oxygen contribution to the DOS for $La_8Ni_4O_{17}$ and the overall oxygen contribution for $La_2NiO_{4.00}$.

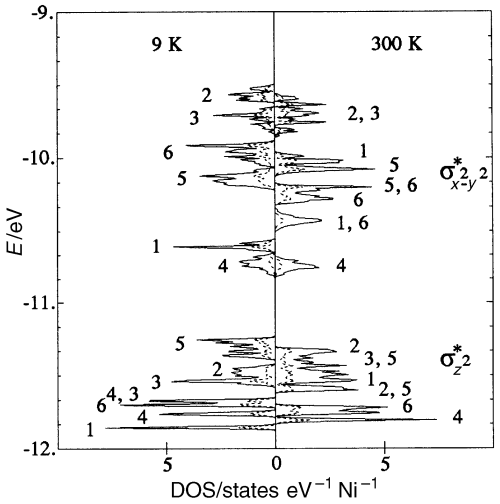

Fig. 2 DOS curves for $La_8Ni_4O_{17}$ at 9 and 300 K, focused on nickel 3d character σ^* bands. Dotted line shows the oxygen contribution to the DOS. Main nickel contributions to the bands are indicated, as labelled in Table 1.

will be seen in the following, to a mixed valence for nickel, including Ni^+. It can be stressed that, in the case of copper(II) derivatives, the distribution of electronic populations can not be so wide because of the higher number of electrons (the σ^* bands stack is 3/4 filled in the case of Cu^{2+}, half-filled in the case of Ni^{2+}); for this reason the stabilisation of such a distorted crystal structure and associated Cu^+/Cu^{3+} mixed valence is less expected in the case of doped copper(II) oxides.

Fig. 3 focuses on oxygen 2p character bands. Interstitial oxygen atoms lead to the formation of very narrow bands, including a significant contribution of apex oxygen atoms, in the range from -15 to -14 eV, *i.e.* above the usual $2p_\pi$ bands. A COOP analysis reveals that these bands are of antibonding character with respect to the $O_{apex}-O_i$ bonds. Corresponding $O_{apex}-O_i$ slightly bonding states are found within the 2p band stack. In addition, the strongly localised character of the antibonding interstitial oxygen bands suggests that a non-negligible oxygen Hubbard parameter U_{pp} should be associated to them. This will be discussed in the next section.

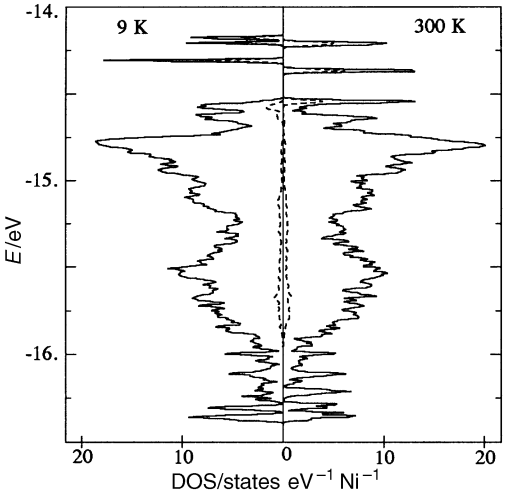

Fig. 3 DOS curves for $La_8Ni_4O_{17}$ at 9 and 300 K, focused on oxygen character bands. Dotted line shows the interstitial oxygen contribution to the DOS.

The main differences between the room- and low-temperature DOS diagrams of $La_8Ni_4O_{17}$ arise from the stabilisation or destabilisation of some $\sigma^*_{z^2}$ and $\sigma^*_{x^2-y^2}$ antibonding bands. Projected DOS (Fig. 2) show that, at increasing temperature, a destabilisation occurs for the Ni(1) $\sigma^*_{z^2}$ and $\sigma^*_{x^2-y^2}$ bands and to a less extent for the Ni(3) $\sigma^*_{z^2}$ bands. A stabilisation occurs for the Ni(6) $\sigma^*_{x^2-y^2}$ bands and to a lesser extent for the Ni(2) $\sigma^*_{x^2-y^2}$ and Ni(5) $\sigma^*_{z^2}$ bands. This is related to the charge transfer or disproportionation equilibrium (1). The total and projected DOS (Fig. 1–3) show that the narrow bands retain a significant covalent character. The term 'localised states' means that the structural distortions split bands into molecular orbitals corresponding to NiO_m and O_3 clusters. The electrons described by these almost non-dispersive bands are delocalised on few atoms (nephelauxetic effect), but localised from the crystal point of view. This is consistent with a hopping-type conductivity in narrow bands.

In order to further discuss the above results we have to locate E_F using experimental data. In addition, the determination of E_F leads to assign electronic configurations to the six types of nickel ions in $La_8Ni_4O_{17}$.

Discussion: determination of the Fermi level position

The Fermi level of $La_8Ni_4O_{17}$ is located in $3d_\sigma^*$ bands, originating mainly from nickel $3d_{z^2}$ and $3d_{x^2-y^2}$ orbitals. The bands narrowness and the projected DOS illustrate the localised character of the corresponding states. As a consequence, the single occupancy of some $3d_\sigma^*$ bands may be energetically favourable with regard to their double occupancy. To each band filling scheme corresponds a given position of the Fermi level.

A correct location of E_F and correct corresponding electronic configurations should account for: (*a*) a smooth dependence between the overlap populations and the Ni—O bond lengths, which are the only ones affected by the partial occupancy of the $3d_\sigma^*$ bands. The larger the cumulated overlap population, the shorter the bond. In other words, electronic and crystallographic structures must be correlated *via* the induced band structure, corresponding electronic configurations and overlap populations. (*b*) States close to E_F involving those nickel ions affected by the charge-transfer equilibrium (1). These states should be also related to the main differences observed between room- and low-temperature band structures. As described in ref. 8, the differences between the room- and low-temperature structures of $La_8Ni_4O_{17}$ were attributed to a shift of the charge-transfer equilibrium (1) between Ni(1), Ni(5) and Ni(6) nickel

ions that are actually involved in the stabilisation or destabilisation of bands between 9 and 300 K. (*c*) The occurrence of a mixed nickel valence (from +I to +III).[7,8] (*d*) A significant enhancement of the Curie constant C_M between 9 and 300 K, corresponding roughly to a higher number of unpaired electrons, *i.e.* of singly occupied bands.

The localised and antibonding character of the O_i bands suggests a significant Hubbard parameter U_{pp} affecting these oxygen-character bands in particular. Depending on the magnitude of U_{pp}, a back-transfer of electrons to the nickel and hence a formal charge of −e instead of −2e for the interstitial oxygen, or the formation of $(O_3)^{5-}$ clusters, can occur. As a matter of fact, U_{pp} values ranging between 4 and 5 eV were previously proposed for copper and vanadium oxides, using various spectroscopic methods.[24–26] The existence of the $(O_3)^{5-}$ species in this material has already been argued in ref. 8 on the basis of bond-order and Madelung potential analysis. From the band structure viewpoint, the $(O_3)^{5-}$ hypothesis gives rise to one more electron in the 3d character bands for one interstitial oxygen atom and the mean formal oxidation state of nickel is lowered by 0.25 (from 2.50 to 2.25).

The band diagrams corresponding to the best agreement with experimental data, assuming the existence of $(O_3)^{5-}$, are given in Fig. 4. The electronic configurations are given in Table 3, and curves of Ni—O bond lengths *vs.* overlap populations, corresponding to these band diagrams, are given in Fig. 5. E_F crosses a few bands at 9 K as well as 300 K, which agrees with the description of the electrical properties in terms of more than one type of carriers in narrow bands.[1] There is a higher number of singly occupied bands at 300 K than at 9 K, accounting for an enhancement of the Curie constant at increasing temperature. As assumed, the nickel ions involved in the charge transfer equilibrium (1) and reflecting the main differences between low- and room-temperature band diagrams are indeed contributing to the bands close to E_F. Monovalent

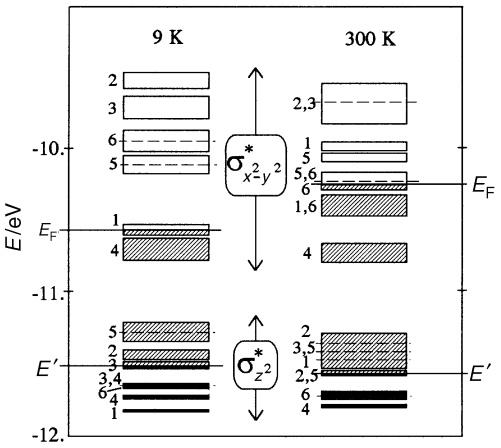

Fig. 4 Band diagrams for $La_8Ni_4O_{17}$ at 9 and 300 K, focused on Ni 3d character σ^* bands, assuming the formation of $(O_3)^{5-}$ species. Main nickel contributions to the bands are indicated, as labelled in Table 1. Dotted lines indicate that two bands overlap. E' indicates the upper level occupied by two electrons. Levels between E' and E_F are singly occupied.

Table 3 Electronic configurations of Ni ions, assuming that interstitial oxygen atoms form O_3^{5-} species

	9 K	300 K
Ni (1):	[Ar] t_{2g}^6 $d_{z^2}^{1.9}$ $d_{x^2-y^2}^{0.5}$	[Ar] t_{2g}^6 $d_{z^2}^{1.1}$ $d_{x^2-y^2}^{0.3}$
Ni (2):	[Ar] t_{2g}^6 $d_{z^2}^{1.2}$ $d_{x^2-y^2}^{0.0}$	[Ar] t_{2g}^6 $d_{z^2}^{1.3}$ $d_{x^2-y^2}^{0.1}$
Ni (3):	[Ar] t_{2g}^6 $d_{z^2}^{1.6}$ $d_{x^2-y^2}^{0.2}$	[Ar] t_{2g}^6 $d_{z^2}^{1.1}$ $d_{x^2-y^2}^{0.1}$
Ni (4):	[Ar] t_{2g}^6 $d_{z^2}^{2.0}$ $d_{x^2-y^2}^{0.6}$	[Ar] t_{2g}^6 $d_{z^2}^{1.9}$ $d_{x^2-y^2}^{0.7}$
Ni (5):	[Ar] t_{2g}^6 $d_{z^2}^{1.1}$ $d_{x^2-y^2}^{0.1}$	[Ar] t_{2g}^6 $d_{z^2}^{1.2}$ $d_{x^2-y^2}^{0.2}$
Ni (6):	[Ar] t_{2g}^6 $d_{z^2}^{1.8}$ $d_{x^2-y^2}^{0.1}$	[Ar] t_{2g}^6 $d_{z^2}^{1.9}$ $d_{x^2-y^2}^{0.5}$

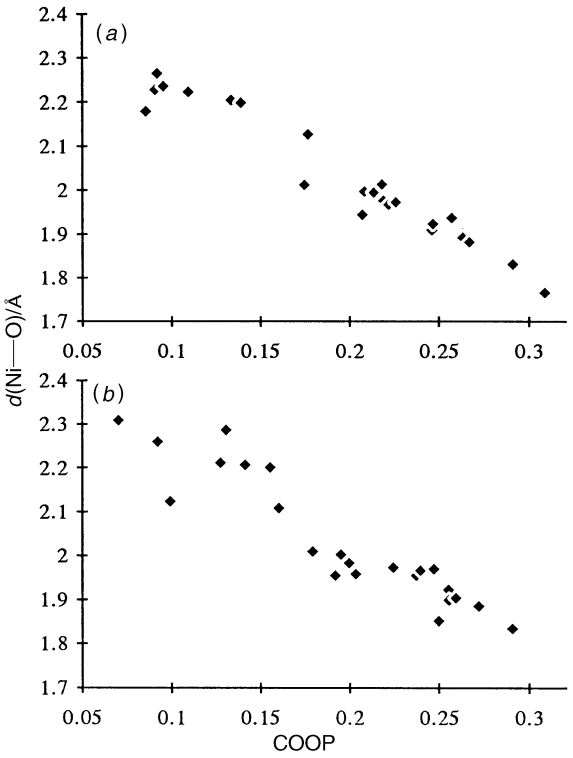

Fig. 5 COOP *vs.* Ni—O distance diagrams for $La_8N_4O_{17}$ at (*a*) 9 K and (*b*) 300 K, assuming that interstitial oxygen atoms form O_3^{5-} species

nickel does occur in each configuration scheme as expected from the EPR and structural studies.[7,8]

A few bands appear to be stabilised within each $\sigma^*_{z^2}$ and $\sigma^*_{x^2-y^2}$ band stacks. As the occupancy of antibonding bands is associated to larger bond lengths, these bands are lowered in energy. For instance, $\sigma^*_{x^2-y^2}$ bands associated with Ni(1) and Ni(4) are clearly stabilised at 9 K, which indicates a higher occupancy. It is important to point out again that the respective energies of the bands within $\sigma^*_{z^2}$ and $\sigma^*_{x^2-y^2}$ stacks are not independent because of the non-negligible overlap between $3d_{z^2}$ and in-plane $2p_\sigma$ atomic orbitals.

Using the same monoelectronic band structures as a starting point, we assumed in a second stage the interstitial oxygen ions to be O^{2-} ions instead of forming $(O_3)^{5-}$ clusters, which corresponds to the above situation, minus one electron per O_i in 3d character bands. A satisfactory fitting with experimental data can be obtained again (Fig. 6 and 7, Table 4). More especially monovalent nickel [Ni(1) and Ni(4)] is still present at 9 and 300 K despite the smaller number of 3d electrons. The bands affected by increasing temperature, associated to Ni(1) and Ni(6), lie close to E_F at 9 K. Ni(1) and Ni(6) are, moreover, involved in the equilibrium (1) whose displacement depends on temperature. Such results suggest that the electron transfer from the interstitial oxygen atoms towards the NiO_2 layers could be not complete.

Conclusion

Extended Hückel band structure calculations have been performed using the actual crystal structure of $La_8Ni_4O_{17}$ at 9 and 300 K, in order to correlate the structural features with the electronic properties of the compound. The band diagrams were built on the basis of the calculated monoelectronic band structures, assuming a rigid band model and discussing the location of the Fermi level in order to fit the experimental data. The obtained band diagrams allow interpretation of the electronic properties of $La_8Ni_4O_{17}$ which can be clearly correlated to its strongly distorted structure. Actually the crystal

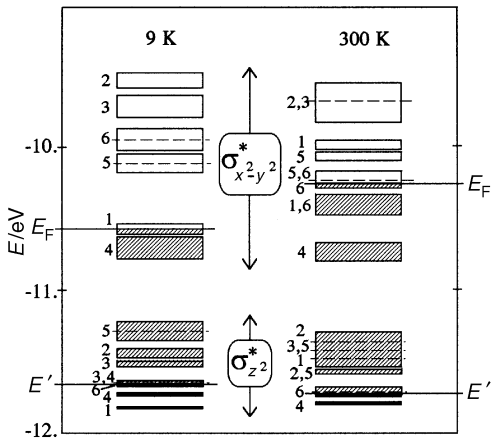

Fig. 6 Band diagrams for $La_8Ni_4O_{17}$ at 9 and 300 K, focused on nickel 3d character σ^* bands, in the O^{2-} interstitial oxygen hypothesis. Main nickel contributions to the bands are indicated, as labelled in Table 1. Dotted lines indicate that two bands overlap. E' indicates the upper level occupied by two electrons. Levels between E' and E_F are singly occupied.

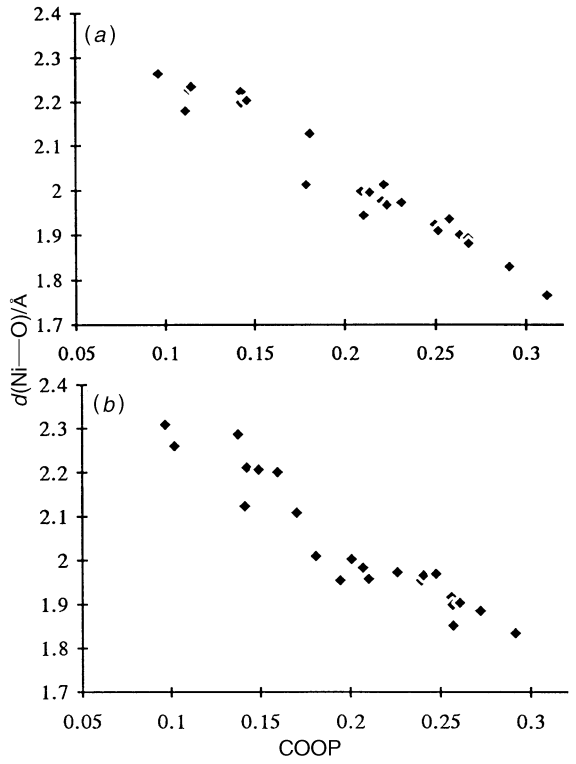

Fig. 7 COOP *vs.* Ni—O distance diagrams for $La_8Ni_4O_{17}$ at (*a*) 9 K and (*b*) 300 K, assuming that interstitial oxygen atoms form O^{2-} species

Table 4 Electronic configurations of Ni ions, assuming that interstitial oxygen atoms form O^2-species

	9 K	300 K
Ni (1):	$[Ar]\ t_{2g}^6\ d_{z^2}^{1.9}\ d_{x^2-y^2}^{0.5}$	$[Ar]\ t_{2g}^6\ d_{z^2}^{1.0}\ d_{x^2-y^2}^{0.3}$
Ni (2):	$[Ar]\ t_{2g}^6\ d_{z^2}^{1.0}\ d_{x^2-y^2}^{0.0}$	$[Ar]\ t_{2g}^6\ d_{z^2}^{1.0}\ d_{x^2-y^2}^{0.1}$
Ni (3):	$[Ar]\ t_{2g}^6\ d_{z^2}^{1.1}\ d_{x^2-y^2}^{0.0}$	$[Ar]\ t_{2g}^6\ d_{z^2}^{1.0}\ d_{x^2-y^2}^{0.1}$
Ni (4):	$[Ar]\ t_{2g}^6\ d_{z^2}^{1.6}\ d_{x^2-y^2}^{0.6}$	$[Ar]\ t_{2g}^6\ d_{z^2}^{1.8}\ d_{x^2-y^2}^{0.7}$
Ni (5):	$[Ar]\ t_{2g}^6\ d_{z^2}^{1.0}\ d_{x^2-y^2}^{0.1}$	$[Ar]\ t_{2g}^6\ d_{z^2}^{1.0}\ d_{x^2-y^2}^{0.2}$
Ni (6):	$[Ar]\ t_{2g}^6\ d_{z^2}^{1.4}\ d_{x^2-y^2}^{0.1}$	$[Ar]\ t_{2g}^6\ d_{z^2}^{1.3}\ d_{x^2-y^2}^{0.5}$

symmetry and bond lengths distribution give rise to a complex splitting of the σ^* bands, each of them being associated with specific nickel sites. Conversely, the unequal occupancy of these bands leads to the stabilisation of different oxidation states for nickel ions. These features result in a semiconducting behaviour and in the occurrence of Ni^+. The formation of Ni^+ ions at low as well as at room temperature can be ascribed to the existence of ordered interstitial oxygen atoms which govern the equilibrium between the crystal and electronic structures, leading to localised cluster states, the Ni—O covalence being preserved.

Band diagrams also corroborate experimental data such as the hopping-type electrical conductivity, as well as the temperature dependence of the Curie constant and of the Ni—O bond lengths distribution. The complex thermal variation of the thermoelectric power[1] can be correlated with the overlap of $\sigma^*_{x^2-y^2}$ and $\sigma^*_{z^2}$ narrow bands at E_F, leading to two types of carriers.

Interstitial oxygen atoms lead to very narrow $O_{apex}—O_i—O_{apex}$ energy bands. These purely oxygen localised states can be associated to a significant Hubbard parameter U_{pp}, supporting the occurrence of $(O_3)^{5-}$ entities in $La_8Ni_4O_{17}$. The existence of only O^{2-} ions at all oxygen sites leads also to a consistent fitting of experimental results, but it seems ruled out on account of the short $O_i—O_{apex}$ bond lengths.[8]

The authors acknowledge L. Ducasse and J. Etourneau for fruitful discussions, the Pôle de Modélisation Intensive (Pôle M.N.I., Université de Bordeaux I) and the Laboratoire de Physicochimie Théorique (UA 503-CNRS, Bordeaux) for computational support.

References

1 A. Demourgues, P. Dordor, J.-P. Doumerc, J.-C. Grenier, E. Marquestaut, M. Pouchard, A. Villesuzanne and A. Wattiaux, *J. Solid State Chem.*, 1996, **124**, 199 and references therein.
2 J. M. Bassat, P. Odier and J.-P. Loup, *J. Solid State Chem.*, 1994, **110**, 124.
3 J. M. Tranquada, D. J. Buttrey, V. Sachan and J. E. Lorenzo, *Phys. Rev. Lett.*, 1994, **73**, 1003.
4 J. M. Tranquada, Y. Kong, J. E. Lorenzo, D. J. Buttrey, D. E. Rice and V. Sachan, *Phys. Rev. B*, 1994, **50**, 6340.
5 K. Yamada, T. Omata, K. Nakajima, Y. Endoh and S. Hosoya, *Physica C*, 1994, **221**, 355.
6 M. J. Sayagués, M. Vallet-Regí, J. L. Hutchison and J. M. González-Calbet, *J. Solid State Chem.*, 1996, **125**, 133.
7 A. Demourgues, A. Wattiaux, J.-C. Grenier, M. Pouchard, J. Soubeyroux, J.-M. Dance and P. Hagenmuller, *J. Solid State Chem.*, 1993, **105**, 458.
8 A. Demourgues, F. Weill, B. Darriet, A. Wattiaux, J.-C. Grenier, P. Gravereau and M. Pouchard, *J. Solid State Chem.*, 1993, **106**, 330.
9 A. Demourgues, F. Weill, B. Darriet, A. Wattiaux, J.-C. Grenier, P. Gravereau and M. Pouchard, *J. Solid State Chem.*, 1993, **106**, 317.
10 V. I. Anisimov, M. A. Korotin, J. Zaanen and O. K. Andersen, *Phys. Rev. Lett.*, 1992, **68**, 345.
11 R. Hoffmann, *J. Chem. Phys.*, 1963, **39**, 1397.
12 J. H. Ammeter, H.-B. Bürgi, J. C. Thibeault and R. Hoffmann, *J. Am. Chem. Soc.*, 1978, **100**, 3686.
13 M.-H. Whangbo and R. Hoffmann, *J. Am. Chem. Soc.*, 1978, **100**, 6093.
14 R. Kasowski and M.-H. Whangbo, *Inorg. Chem.*, 1990, **29**, 360.
15 R. Hoffmann, *Solids and Surfaces: A Chemist's View of Bonding in Extended Structures*, VCH, New York, 1988.
16 E. Canadell and M.-H. Whangbo, *Chem. Rev.*, 1991, **91**, 965.
17 J. K. Burdett and S. A. Gramsh, *Inorg. Chem.*, 1994, **33**, 4309.
18 J. K. Burdett, *Chemical Bonding in Solids*, Oxford University Press, New York, 1995.
19 A. Villesuzanne and M. Pouchard, *C. R. Acad. Sci. Paris, Sér. II*, 1996, **310**, 155.
20 T. Hughbanks and R. Hoffmann, *J. Am. Chem. Soc.*, 1983, **105**, 3528.
21 R. S. Mulliken, *J. Chem. Phys.*, 1955, **23**, 1833.
22 M. Evain, M.-H. Whangbo, A. Ben Salem and A. Meerschaut, *Solid State Commun.*, 1989, **72**, 971.
23 M.-H. Whangbo, *J. Chem. Phys.*, 1979, **70**, 4963.
24 G. A. Sawatsky and D. Post, *Phys. Rev. B*, 1979, **20**, 1546.
25 D. van der Marel, J. van Elp, G. A. Sawatsky and D. Heitmann, *Phys. Rev. B*, 1988, **37**, 5136.
26 J. Ghijsen, L. H. Tjeng, J. van Elp, H. Eskes, J. Westerink, G. A. Sawatsky and M. T. Czyzyk, *Phys. Rev. B*, 1988, **38**, 11322.

Paper 6/07240B; *Received* 23*rd October*, 1996